Quantum-mechanical calculation of multiple electron removal and fragmentation cross sections in He^+-H_2O collisions

Mitsuko Murakami,* Tom Kirchner,† and Marko Horbatsch
Department of Physics and Astronomy, York University, Toronto, Ontario, Canada M3J 1P3

Hans Jürgen Lüdde
Institut für Theoretische Physik, Goethe-Universität, D-60438 Frankfurt, Germany

(Received 30 July 2012; published 31 August 2012)

Electron removal and fragmentation cross sections are calculated for $He^+(1s)$-H_2O collisions at impact energies from 20 keV/amu to several MeV/amu by using the nonperturbative basis generator method for ion-molecule collisions. Previous work for proton impact is extended to deal with the dressed projectile in the present case. The effects from the active projectile electron are taken into account by applying the same single-particle Hamiltonian to all electrons and by using the inclusive-probability formalism in the final-state analysis. Fragment-ion yields are evaluated from the single-, double-, and triple-electron removal cross sections, and the results are compared with the available experimental data. Very reasonable agreement is obtained for fragmentation caused by direct ionization, while some discrepancies remain in the capture and loss data.

DOI: 10.1103/PhysRevA.86.022719 PACS number(s): 34.10.+x, 34.50.Gb, 34.70.+e

I. INTRODUCTION

Fragmentation of water molecules induced by ion impact has been the subject of active research in the last 15 years. The pioneering work by Werner *et al.* [1] was followed up by Gobet *et al.* [2], who measured the fragmentation cross sections in proton-water vapor collisions for 15–100 keV impact energies. A time-of-flight coincidence technique was used to record different fragment ions (H_2O^+, OH^+, H^+, O^+, and O^{2+}) separately, as well as the final charge state of the incident proton, providing detailed information about the fragmentation channels. A series of measurements for different projectiles was carried out in the following years by various groups, for example, for Ne^{q+} (q = 1,3,5,7,9) [3], C^{3+}, O^{5+} [4], and He^{2+} [5–7] ions, for atomic hydrogen [8,9], electrons [10], C^0 atoms and C^+ ions [11], for protons (with extended impact energies above 500 keV) [9], and for He^+ ions [12]. Of particular interest for us are the experiments with dressed projectiles (e.g., He^+) which carry an additional electron into the collision to participate in the charge-transfer processes. In such cases, the cross section for the projectile-electron loss channel was also measured to complete the picture.

Prior to these experiments, Tan *et al.* [13] reported the branching ratios of water fragmentation using fast (several keV) electron impact in the Bethe-Born regime, in which the results can be considered equivalent to those of photoionization experiments. They measured both molecular orbital (MO)-specific vacancy production and ionic fragment yields, and derived fragmentation branching ratios, which are deemed to be independent of the details of the collision dynamics such as impact energy, charge state of the projectile, or multiplicity of the target ionization.

In this paper, we report on calculations of the cross sections for the various electron removal processes in He^+–H_2O collisions using the recently proposed independent-particle model basis generator method (IPM-BGM) adapted for ion-molecule collisions [14]. In Refs. [15,16] we demonstrated that multiple-electron removal in proton-water collisions can be understood using this approach, and that a fragmentation model valid over a wide range of energies can be built upon the calculated electron removal cross sections. The above-mentioned branching ratios of Tan *et al.* were shown to not be sufficient to explain fragmentation in intermediate- and low-energy collisions due to the increasing importance of multi-electron removal processes.

The fragmentation model validated for proton-H_2O collisions [15,16] is used to determine the fragment-ion yields after He^+ impact on the basis of calculated single-, double-, and triple-electron removal cross sections, and the results are compared with the experimental data of Garcia *et al.* [12].

In comparison with the proton projectile case [15,16], calculations for the He^+ projectile are complicated by the fact that the additional projectile electron can take part in charge-transfer processes, and should be treated on an equal footing as the N target electrons. In this work, this is accomplished by propagating the projectile electron simultaneously with the target electrons using the same single-particle Hamiltonian and basis, and by using the inclusive-probability formalism [17] in the final-state analysis. As a consequence, the effect of Pauli blocking in the electron transfer from the target to the He^+ projectile is described properly since inclusive probabilities are derived from antisymmetric wave functions of the $(N+1)$-electron system [18,19].

The paper is organized as follows. In Sec. II A, we describe the IPM-BGM approach to He^+–H_2O collisions. The computation of charge-state correlated probabilities of single- and multiple-electron removal from the properly antisymmetrized wave functions using the inclusive-probability formalism is explained in Sec. II B, and a set of equations for the

*Present address: Center for Quantum Science and Engineering, Department of Physics, National Taiwan University, Taipei 10617, Taiwan.
†tomk@yorku.ca

fragmentation cross sections is introduced in Sec. II C. Results are presented in Sec. III, followed by conclusions in Sec. IV. Atomic units ($\hbar = m_e = e = 4\pi\epsilon_0 = 1$) are used throughout, unless specified otherwise.

II. THEORY

A. IPM-BGM formulation of ion-molecule collisions

The theoretical formulation of the He^+–H_2O collision problem is similar to the one we used for proton-H_2O collisions [15], which is why we only give a brief summary highlighting the extensions for the treatment of a dressed projectile. We assume that at impact energies $E_P \geqslant 20$ keV/amu the projectile moves on a classical straight-line trajectory, while the target molecule is fixed in space during the collisional interaction. Furthermore, we assume that the (nonrelativistic) electronic Hamiltonian is of single-particle form (i.e., we model the interelectronic Coulomb repulsion by effective potentials). The task within this IPM description is to solve a set of time-dependent Schrödinger equations

$$i\,\partial_t \left|\psi^j_{\alpha\beta\gamma}(t)\right\rangle = \hat{H}_{\alpha\beta\gamma}(t)\left|\psi^j_{\alpha\beta\gamma}(t)\right\rangle, \quad j = 1,\ldots,N+1, \quad (1)$$

for the initially occupied orbitals on the target *and* the projectile. The orientation of the molecule relative to the projectile beam direction is specified by the Euler angles α, β, γ. As in our previous works we consider two different orientations and approximate the fully angle-averaged total cross sections for all electronic processes considered as the averages of just these two orientations [14,15].

For He^+–H_2O collisions, there are five doubly occupied MOs at the target and one singly occupied atomic orbital (AO) at the projectile. In practice, the innermost MO ($1a_1$) of the H_2O molecule is assumed frozen in the present calculation since inelastic transitions from $1a_1$ are negligibly small compared to the more weakly bound orbitals [15,16]. The single-particle Hamiltonian in Eq. (1) can be expressed as

$$\hat{H}_{\alpha\beta\gamma} = \hat{H}^T_{\alpha\beta\gamma} + V^P \quad (2)$$

with an effective target Hamiltonian $\hat{H}^T_{\alpha\beta\gamma}$ and an effective projectile potential V^P. For $\hat{H}^T_{\alpha\beta\gamma}$ we use an energy representation of a minimal-basis-set ground-state Hartree-Fock (HF) description of H_2O [20], while the projectile potential is taken to be of the form

$$V^P(r_P) = -\frac{Z_P}{r_P} + \int \frac{\left|\psi^{\rm He}_{1s}(r)\right|^2}{|\mathbf{r}-\mathbf{r}_P|} d^3r\,, \quad (3)$$

in which $\psi^{\rm He}_{1s}$ is the (normalized) ground-state HF AO of neutral helium, $\mathbf{r}_P$ the position vector of the electron with respect to the projectile center, and $Z_P = 2$.

This choice of Hamiltonian $\hat{H}_{\alpha\beta\gamma}$ describes the situation for an initial target electron before the collision properly: The electron is bound in an (HF) eigenstate of neutral H_2O represented in terms of $1s$, $2s$, and $2p$ Slater-type orbitals (STOs) on the oxygen center and $1s$ STOs on both hydrogen centers [20], and it experiences an asymptotic $-1/r_P$ potential due to the incoming He^+ projectile. However, the situation is somewhat different for the initial projectile electron: In reality, it is exposed to a bare Coulomb potential corresponding to $Z_P = 2$ and a short-range potential of the distant neutral water molecule, whereas in our description it occupies a neutral-helium HF orbital and experiences a long-range target potential. This shortcoming cannot be remedied easily unless one abandons the idea to describe the $(N+1)$-electron system in terms of one common single-particle Hamiltonian. One then would have to deal with nonorthogonal propagated target and projectile orbitals and possibly significant overlaps at the final time t_f, at which the analysis is to be performed [18,21]. The present scheme preserves orthogonality at all times such that the final-state analysis remains straightforward [19]. One can expect that it gives a reasonable account of electron transfer processes from the target to the continuum and to the projectile, but may have limitations in the description of projectile electron loss. If one were to emphasize the latter process, one would choose a different Hamiltonian, which would probably imply a compromised description of capture and target ionization.

We have solved the single-particle equations (1) with the molecular IPM-BGM. The gist of this method is a single-center expansion of the initially populated MOs which are used in the spectral representation of $\hat{H}^T_{\alpha\beta\gamma}$ and a two-center BGM representation of the propagated orbitals. This turns Eqs. (1) into coupled-channel equations, which are similar to those of an ion-atom collision problem and, in particular, are not plagued by the occurrence of multicenter matrix elements. For the results presented below we have used the same techniques and parameters as described in Ref. [15].

B. Analysis of electron transfer processes

We treat the collision system in such a way that all electrons are indistinguishable at the end of the collision, no matter whether they belonged to the water molecule or to the He^+ projectile before the collision. The number of electrons considered active in the water molecule is $N = 8$, and thus we are dealing with an $N+1 = 9$-electron system. The main ingredient of the final-state analysis is the one-particle density matrix at $t = t_f$

$$\langle f|\hat{\gamma}^1(t_f)|f'\rangle = \sum_{j=1}^{N+1} \left\langle f\left|\psi^j_{\alpha\beta\gamma}(t_f)\right\rangle\right\langle\psi^j_{\alpha\beta\gamma}(t_f)\left|f'\right\rangle, \quad (4)$$

which is composed of single-particle amplitudes for the transitions of the $(N+1)$ mutually orthogonal propagated states $|\psi^j_{\alpha\beta\gamma}(t_f)\rangle$ to the final states $|f\rangle$. It was explained in previous works how the exclusive and inclusive probabilities for ionization and electron transfer processes can be extracted from Eq. (4) in a way that is consistent with the assumption that the propagated many-electron state as well as the final states of interest are restricted to single Slater determinants (see Refs. [15,17,18], and specifically Eqs. (18) to (20) of Ref. [21], which are used to obtain charge-state correlated probabilities). We will not repeat this discussion here, but note that we have performed the inclusive-probability analysis for both ion-molecule orientations considered (i.e., all cross sections reported below are minimal orientation-averages as introduced in Refs. [14,15]).

Following the determinantal inclusive analysis of the final states, the charge-state correlated cross sections $\sigma_{k,l}$ for $l = 0,1,\ldots$ electrons found in the continuum, with $k = 0,1,2$

electrons found on the projectile after the collision, can be classified as (i) loss ($k = 0$), (ii) pure ionization ($k = 1$), and (iii) capture ($k = 2$). We note, however, that this is an approximate identification since the projectile electron is not passive in our approach.

One can define partial net cross sections σ_k, which are labeled by a single index k ($= 0,1,2$). The process where a neutral projectile emerges irrespective of the number of electrons found in the continuum is defined by $k = 2$ and a sum over $l = 0,1,\ldots,N-1$

$$\sigma_2 = \sum_{l=0}^{N-1} \sigma_{2,l} \,. \tag{5}$$

This cross section should be equal to the single-electron capture cross section in Refs. [22–24], which was denoted as σ_{10} in those works. We also evaluate the weighted sum

$$\tilde{\sigma}_2 = \sum_{l=0}^{N-1} (l+1)\sigma_{2,l} \tag{6}$$

for a comparison with the sum of the four dominant singly charged fragment ion yields in the capture channel of Ref. [12].

The partial net cross section where the projectile emerges in the same charge state (predominantly the pure ionization cross section) corresponds to $k = 1$, and $l = 0,1,\ldots,N$ electrons in the continuum

$$\tilde{\sigma}_1 = \sum_{l=1}^{N} l\sigma_{1,l} \,, \tag{7}$$

where, as in Eq. (6), we use the tilde to indicate that the sum is weighted. This cross section should be equal to the sum of the four singly charged fragment ion yields reported in the pure ionization channel of Ref. [12]. In addition, we calculate the cross section for net free-electron production (σ_-) as

$$\sigma_- = \sum_{k=0}^{2} \sum_{l=1}^{N+1-k} l\sigma_{k,l} \tag{8}$$

for a comparison with the measurements in Refs. [22–24]. Note that using this equation instead of simply summing up all single-particle contributions to free electron production as done in Ref. [19] amounts to assuming that $\sigma_{k,l} = 0$ for $k \geqslant 3$ (i.e., that negative helium ion production does not occur). This cannot be guaranteed in an IPM, and accordingly the present results are not identical to those of Ref. [19]. However, the differences are small since the Pauli principle allows only two electrons with antiparallel spins to populate the projectile's K shell, and transitions to excited single-particle states are unlikely except at the lowest impact energies considered. The situation is similar for the net recoil-ion production cross section discussed at the end of Sec. III A.

Finally, we define the partial net cross section with $l + 1 = 1,2,\ldots,N+1$ electrons in the continuum, and a bare He^{2+} nucleus ($k = 0$) emerging from the collision

$$\sigma_0 = \sum_{l=1}^{N+1} \sigma_{0,l} \,, \tag{9}$$

which should be equal to the He^{2+} production cross section reported by the authors of Refs. [22–24] and denoted as σ_{12} in those works. Furthermore, we also evaluate the weighted sum

$$\tilde{\sigma}_0 = \sum_{l=2}^{N+1} (l-1)\sigma_{0,l} \tag{10}$$

for comparisons with the sum of singly charged fragment ion yields in the loss channel of Ref. [12].

C. Fragmentation products

To account for their experimental data of water fragmentation by dressed projectiles (C^{3+} and O^{5+}), Luna and Montenegro [4] derived a set of empirical equations in terms of the net single- and double-electron removal cross sections. In analogy to their approach, we calculate the fragmentation as [16]

$$\begin{aligned} \sigma_{H_2O^+} &= 0.68\sigma_S \,, \\ \sigma_{OH^+} &= 0.16\sigma_S + 0.6\sigma_D \,, \\ \sigma_{H^+} &= 0.13\sigma_S + 1.2\sigma_D + 2.0\sigma_T \,, \\ \sigma_{O^+} &= 0.03\sigma_S + 0.2\sigma_D + 1.0\sigma_T \,, \end{aligned} \tag{11}$$

where we define the net single-, double-, and triple-electron removal cross sections as

$$\begin{aligned} \sigma_S &= \sigma_{2,0} + \sigma_{1,1} + \sigma_{0,2} \,, \\ \sigma_D &= \sigma_{2,1} + \sigma_{1,2} + \sigma_{0,3} \,, \\ \sigma_T &= \sigma_{2,2} + \sigma_{1,3} + \sigma_{0,4} \,. \end{aligned} \tag{12}$$

For channel-specific fragmentation calculations, we use the following.

(1) Capture channel:

$$\sigma_S^{\rm cap} = \sigma_{2,0} \,, \quad \sigma_D^{\rm cap} = \sigma_{2,1} \,, \quad \sigma_T^{\rm cap} = \sigma_{2,2} \,. \tag{13}$$

(2) Pure ionization channel:

$$\sigma_S^{\rm ion} = \sigma_{1,1} \,, \quad \sigma_D^{\rm ion} = \sigma_{1,2} \,, \quad \sigma_T^{\rm ion} = \sigma_{1,3} \,. \tag{14}$$

(3) Loss channel:

$$\sigma_S^{\rm loss} = \sigma_{0,2} \,, \quad \sigma_D^{\rm loss} = \sigma_{0,3} \,, \quad \sigma_T^{\rm loss} = \sigma_{0,4} \,. \tag{15}$$

III. RESULTS AND DISCUSSION

A. Charge-state correlated cross sections

In Fig. 1 we compare our cross sections with experimental data for the (so-called) capture channel where two electrons are found on the projectile. The net cross section (σ_2) given by Eq. (5) is shown as a solid line and agrees very well with the data of Rudd *et al.* [22] (up to 100 keV/amu). We do not show theoretical data below 20 keV/amu since we are not satisfied with numerical stability in this regime. For energies above 100 keV/amu no direct experimental data are available, and therefore we include results for molecular hydrogen and oxygen targets [23,24], which can be combined according to $\sigma_2(H_2O) = \sigma_2(H_2) + \sigma_2(O_2)/2$ (Bragg additivity rule). These data match well with the measurements for water molecules at 100 keV/amu. Our calculations display a similar shape to the experimental data, except that they appear to be high (by a factor of about 1.5–2). This may be considered not too serious a discrepancy since some of it may be caused by the simple Bragg rule itself.

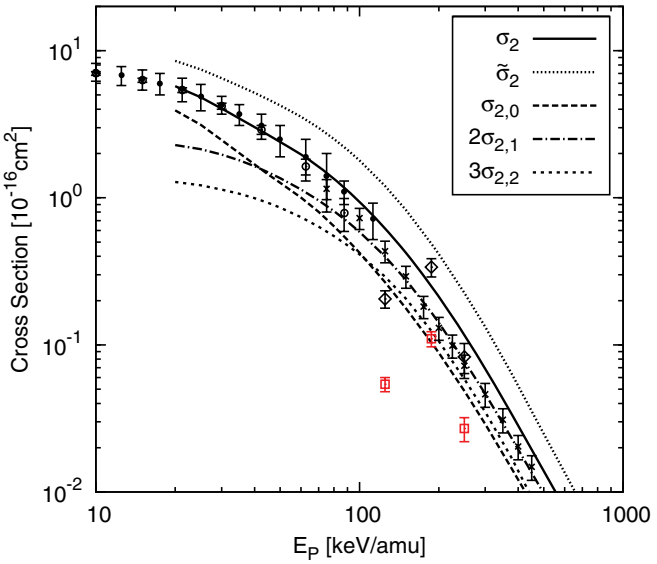

FIG. 1. (Color online) Cross sections associated with $k = 2$ projectile electrons in He^+–H_2O collisions obtained from the inclusive-probability analysis. Shown by solid and dotted lines, respectively, are the net cross sections σ_2 and $\tilde{\sigma}_2$, given by Eqs. (5) and (6). Also shown are the charge-number weighted cross sections for pure single-electron capture ($\sigma_{2,0}$), transfer ionization ($\sigma_{2,1}$), and triple-electron removal where one of the electrons is transferred to the projectile ($\sigma_{2,2}$), which are used to calculate the fragmentation cross sections. Experimental data are for net capture (σ_{10}): (•) [22], (○) [23], and (×) [24]; and for fragment-ion production in the capture channel of Ref. [12]: H_2O^+ ion (□), and the sum of all the fragment ions $\{H_2O^+, OH^+, H^+, O^+, O^{2+}\}$ (◊). Note that the data from Refs. [23,24] are obtained by using the additivity rule $\sigma(H_2) + \sigma(O_2)/2$.

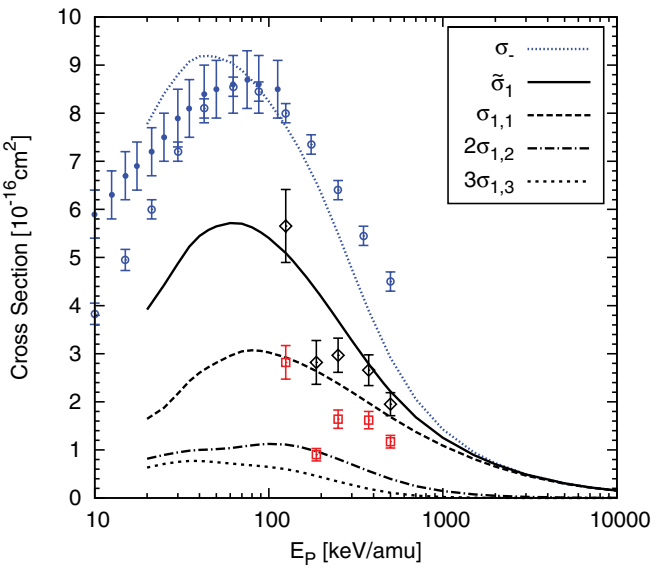

FIG. 2. (Color online) Cross sections associated with $k = 1$ projectile electrons in He^+–H_2O collisions obtained from the inclusive-probability analysis. Shown by the solid line is the pure ionization cross section ($\tilde{\sigma}_1$) given by Eq. (7), and below are the charge-number weighted cross sections for pure single ionization ($\sigma_{1,1}$), pure double ionization ($\sigma_{1,2}$), and pure triple ionization ($\sigma_{1,3}$), which are used to calculate the fragmentation cross sections. Also shown (in blue) is the net free electron yield σ_- given by Eq. (8). Experimental data are for σ_-: (•) [22], (○) [23]; and for the singly charged fragment ion production in the pure-ionization channel of Ref. [12]: H_2O^+ ion (□), and the sum of the four singly charged ions $\{H_2O^+, OH^+, H^+, O^+\}$ (◊). The data from Ref. [23] are obtained by using the additivity rule $\sigma(H_2) + \sigma(O_2)/2$.

Also included in Fig. 1 is the positive ion production cross section ($\tilde{\sigma}_2$) given by Eq. (6), which should correspond to the sum of all the singly charged fragments in the $k = 2$ channel of Garcia *et al.* [12]. The energy dependence of the three available data points (shown as diamonds in the 125–250 keV/amu energy range) in Ref. [12] is unusual, and therefore we conclude that there are probably substantial issues with the overall normalization of these data.

In addition, we show in Fig. 1 how our net cross section is made up from its main three contributions: $\sigma_{2,0}$, $\sigma_{2,1}$, and $\sigma_{2,2}$. For energies below 50 keV/amu, the dominating channel is pure single capture $\sigma_{2,0}$; at higher energies the relative strength of transfer ionization processes becomes evident. Our calculation allows for full electron exchange between projectile, target, and continuum space. Thus, it is possible in principle that the projectile electron was lost, but two electrons were captured to produce the $k = 2$ projectile state. In the inclusive determinantal analysis we have no easy identification method for the strength of such multiple-electron exchange contributions.

The yield for the H_2O^+ ion in the $k = 2$ channel of Ref. [12] is shown in Fig. 1 since it ought to provide a lower bound for $\sigma_{2,0}$. The theoretical calculation touches this bound at 187.5 keV/amu, but this may be related to the experimental issues in the work of Ref. [12] (cf. Fig. 4 and the above discussion of the total positive-ion yield).

In Fig. 2 we show cross sections associated with free-electron production in the continuum. Note that the vertical axis is linear. The solid line represents the net free-electron production cross section for the $k = 1$ channel ($\tilde{\sigma}_1$) as given by Eq. (7). The sum over the fragment yields in the ionization channel of Garcia *et al.* [12] is close to our $\tilde{\sigma}_1$. The H_2O^+ ion yields in Ref. [12] should be a lower bound to the $\sigma_{1,1}$ cross section. In the Bethe-Born limit, $\sigma_{H_2O^+}$ should account for 68% of $\sigma_{1,1}$ [16]. We find that this is satisfied for the two highest of the five data points from Ref. [12]. In addition, we show in the graph how higher-multiplicity events contribute to the net electron production in the $k = 1$ channel. It is remarkable that for 20–40 keV/amu contributions from $\sigma_{1,3}$ become almost competitive with those from $\sigma_{1,2}$ when the electron multiplicity factor is included.

Also shown in Fig. 2 is the net free-electron production cross section σ_- given by Eq. (8). Above 2 MeV/amu the $k = 0,2$ contributions become negligible, and σ_- merges with $\tilde{\sigma}_1$. At low energies (10–120 keV/amu) the experimental σ_- for the water molecule [22] are higher than those obtained with the Bragg additivity rule from the molecular hydrogen and oxygen results [23]; both sets of data support a maximum in the 70–110 keV/amu energy range. Our theoretical calculation, on the other hand, peaks around 30–60 keV/amu. It is possible that better agreement at these energies could come from an inclusion of dynamical screening effects.

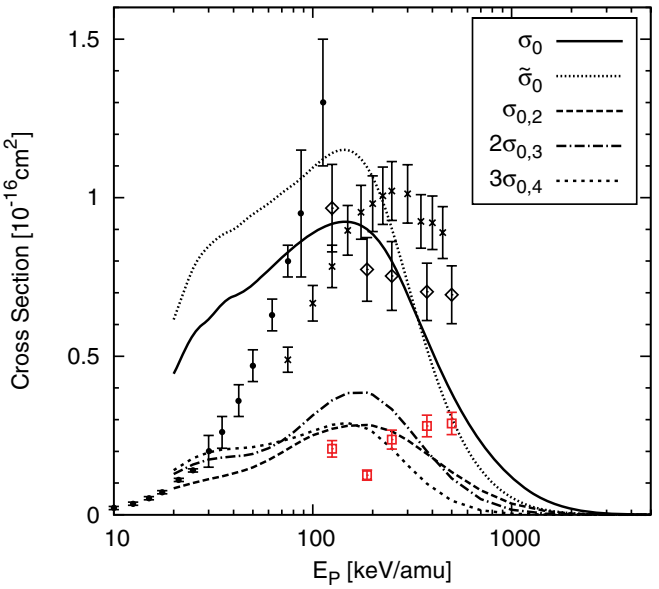

FIG. 3. (Color online) Cross sections associated with $k = 0$ projectile electrons in He^+–H_2O collisions obtained from the inclusive-probability analysis. Shown by the solid and dotted lines, respectively, are the net cross sections σ_0 and $\tilde{\sigma}_0$ given by Eqs. (9) and (10). Also shown are the charge-number weighted cross sections for single removal ($\sigma_{0,2}$), double removal ($\sigma_{0,3}$), and triple removal ($\sigma_{0,4}$) of target electrons in coincidence with projectile electron loss, which are used to calculate the fragmentation cross sections. Experimental data are for He^{2+} production (σ_{12}): (•) [22], (×) [24]; and for positive-ion production in the loss channel of Ref. [12]: H_2O^+ ion (□), and the sum of all the fragment ions $\{H_2O^+, OH^+, H^+, O^+, O^{2+}\}$ (◇). The net loss data from Ref. [24] are obtained by using the additivity rule $\sigma(H_2) + \sigma(O_2)/2$.

In Fig. 3 we consider the projectile electron loss channel. The experimental data from Ref. [22] rise for energies up to 110 keV/amu. The Bragg additivity rule results from the molecular hydrogen and oxygen data in Ref. [24] are seen to be somewhat lower and indicate that a maximum occurs in this net electron production cross section between 200 and 300 keV/amu. The present theoretical data rise too quickly at low energies and display a sharper fall-off above 200 keV/amu. This shortcoming can be explained in the following way: The maximum of a total ionization cross section is known to appear roughly at an impact energy at which the projectile speed is comparable with the average orbital velocity of the electron to be ionized [25]. In the present model we assumed the neutral-He HF potential at the projectile [cf. Eq. (3)] to treat the $(N + 1)$-electron system with a single Hamiltonian. As a result, the binding for the $He^+(1s)$ electron is too weak and the entire cross section appears to be shifted to lower energies on the logarithmic energy scale.

Electron loss occurs in small-to-intermediate impact parameter collisions. Such collisions are dominated by multiple-electron processes. Thus, it appears reasonable that our net electron production cross section is made up of comparable contributions from single-, double-, and triple-electron removal from the water molecule (as shown in Fig. 3).

Concerning the lower bound for the single-electron removal set by the H_2O^+ production cross sections of Garcia *et al.* [12], the three lowest-energy data are below our $\sigma_{0,2}$ as they should. At 400 keV/amu and higher they continue to rise, while the theoretical calculation falls off. This is probably caused by the so-called antiscreening process, which is not taken into account in the IPM-BGM calculations. Antiscreening is a (first-order) mechanism, in which the projectile electron interacts directly with one of the target electrons with the result that both end up in the continuum [26].

The comparison of our $\tilde{\sigma}_0$ [Eq. (10)] and the net fragment-ion yield of Garcia *et al.* [12] shows that the theoretical finding of a strong multiple-ionization contribution in the loss channel is supported by the experiment. The fact that at high impact energies $\tilde{\sigma}_0$ falls below σ_0 is due to projectile electron loss without target ionization, which does contribute to σ_0, but not to $\tilde{\sigma}_0$ [cf. Eqs. (9) and (10)]. Obviously, this process is not measured in experiments, which are based on coincidences with charged fragment ions, but it was extracted from previous measurements for similar ion-atom collision systems by subtracting coincidence cross sections from separately measured total loss cross sections [21]. It would be interesting to see such data also for the present system as this process cannot be caused by antiscreening.

In Fig. 4 we present the cross sections for single-, double-, and triple-electron removal as given by Eqs. (12), which are irrespective of the final projectile charge state. The projectile electron loss channel for which our calculations exhibited some problems in Fig. 3 makes a relatively small contribution. The IPM prediction for σ_T obeys the lower bound set by the H_2O^+ data from Ref. [12] rather well with the exception of the 187.5 keV/amu data point. The present calculation for σ_D falls off more rapidly than σ_S at high energies. In reality this may

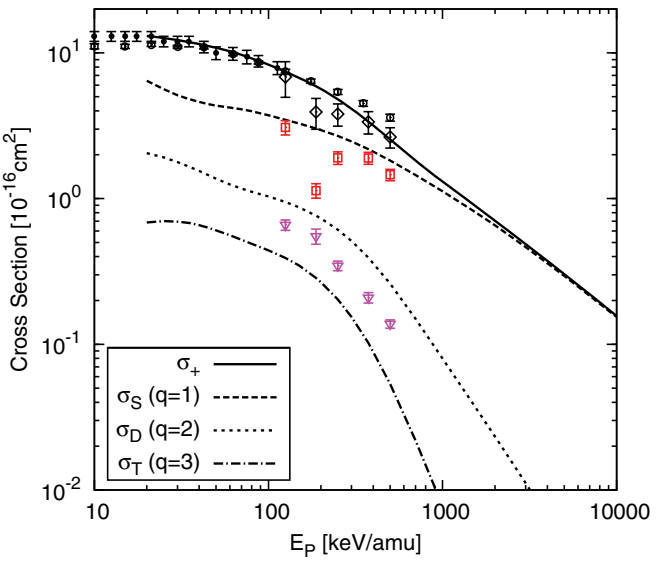

FIG. 4. (Color online) Cross sections for q-fold target electron removal ($\sigma_{S,D,T}$) in proton-H_2O collisions given by Eqs. (12). The solid line at the top displays the net recoil-ion production cross section σ_+ given by Eq. (16). Experimental data are shown for σ_+: (•) [22], (○) [23]; and for the production of singly charged fragment ions in the combined capture, pure ionization, and projectile loss channels of Ref. [12]: H_2O^+ (□), O^+ (▽), and the sum of all the four singly charged ions (◇). The data from Ref. [23] are obtained by using the additivity rule $\sigma(H_2) + \sigma(O_2)/2$.

be different, namely inner-MO single-vacancy production can result in Auger processes [27], in which case the true fall-off will follow that of σ_S.

Interestingly, the production of O^+ as reported in the experiment of Ref. [12] follows a pattern that is similar to both σ_D and σ_T in the 100–500 keV/amu energy range in Fig. 4. In analogy to the proton-H_2O coincidence measurements of Werner *et al.* [1] we would expect σ_T to be dominated by the $H^+ + H^+ + O^+$ reaction. The pattern of the O^+ data from Ref. [12] suggests that they are both associated with the $q = 2$ and $q = 3$ electron removal processes.

Also shown in Fig. 4 at the top is the net recoil-ion production cross section σ_+, given by

$$\sigma_+ = \tilde{\sigma}_2 + \tilde{\sigma}_1 + \tilde{\sigma}_0 = \sigma_2 + \sigma_- - \sigma_0 \,. \tag{16}$$

We observe excellent agreement with Refs. [22,23] for the 20–500 keV/amu energy range. The agreement with the net fragment-ion data of Garcia *et al.* [12] is also excellent except at 187.5 and 200 keV/amu.

B. Fragmentation cross sections

In Fig. 5 we compare our fragmentation model given by Eqs. (11) with the data of Garcia *et al.* [12], where the experimental data are summed over all ($k = 0,1,2$) channels. Except for the energy of 187.5 keV/amu, for which the experimental data display an unusual behavior, we find that theory and experiment are in remarkable agreement. The energy range was shown in Fig. 4 to represent a cross-over regime, where with increasing collision energy the $q > 1$ contributions become less important. We note that in comparison with the proton-H_2O case (cf. Fig. 8 of Ref. [15]) the fragmentation

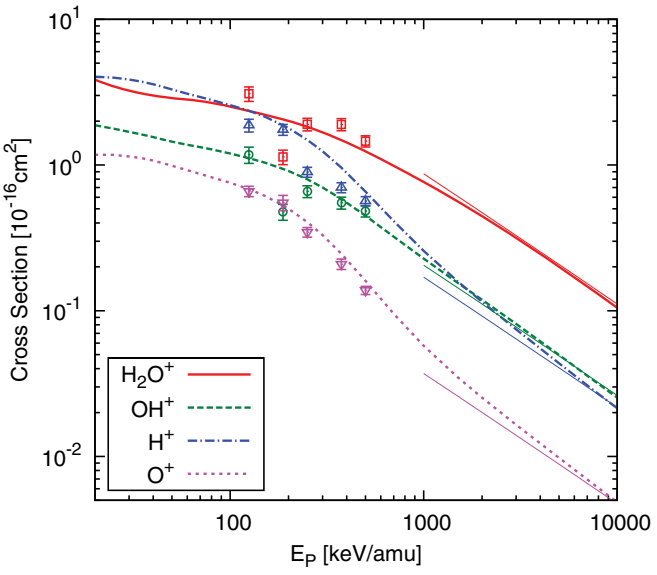

FIG. 5. (Color online) Fragmentation cross sections given by Eqs. (11). The experimental data are obtained as the sum of capture, pure ionization, and loss channels for each fragmentation product in Ref. [12]. The fine solid lines above 1 MeV/amu impact energy represent the Bethe-Born limit (from top to bottom: H_2O^+, OH^+, H^+, and O^+). Experimental data are shown for the production of singly charged fragment ions in the combined capture and ionization channels of Ref. [12]: H_2O^+ (□), OH^+ (◯), H^+ (△), and O^+ (▽).

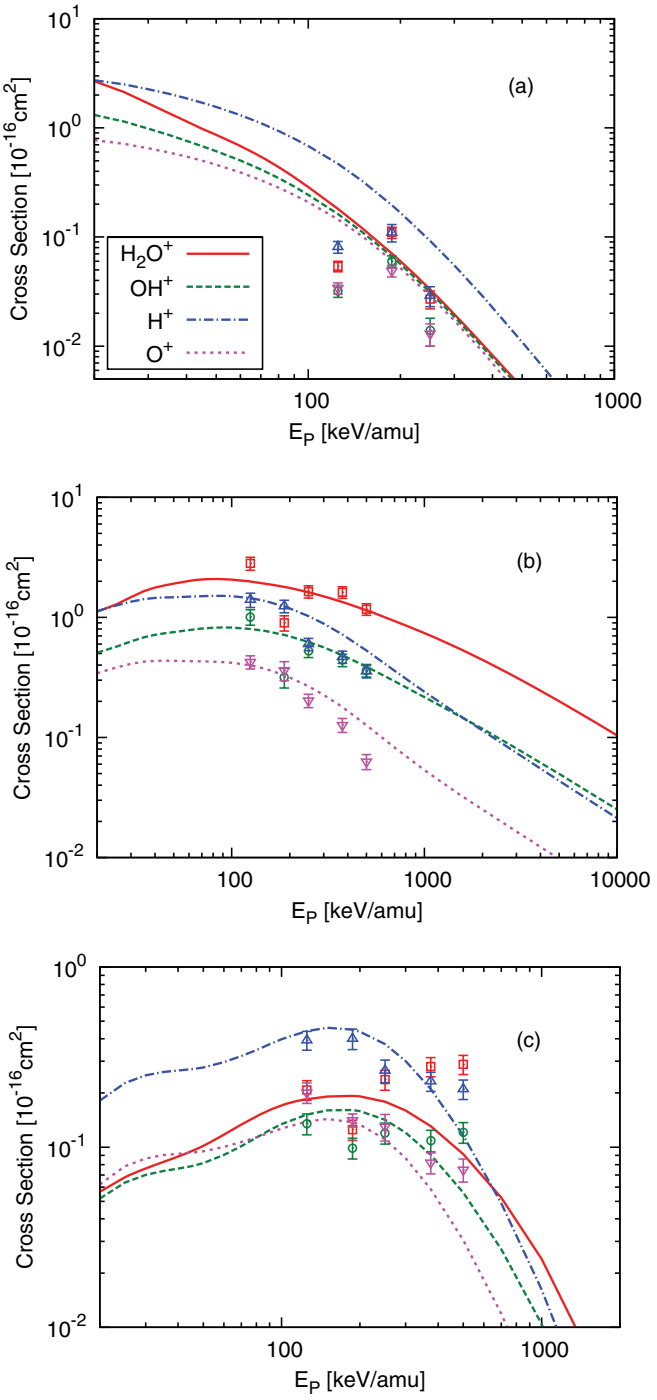

FIG. 6. (Color online) Fragmentation cross sections given by Eqs. (11) for (a) capture, (b) ionization, and (c) projectile loss in He^+–H_2O collisions, according to Eqs. (13), (14), and (15), respectively. The experimental data are from Ref. [12]: H_2O^+ (□), OH^+ (◯), H^+ (△), and O^+ (▽).

cross sections are more compressed. The crossing point for H^+ versus OH^+ productions which occurred in the proton impact case at around 500 keV/amu has moved up to over 1 MeV/amu. This is a consequence of the stronger perturbation by the He^+ projectile causing more multiple ionization.

At low energies ($E_P < 100$ keV/amu), one observes that the H^+ yield becomes competitive with the H_2O^+ production

that is exclusively due to single-electron removal. In the proton impact case the H^+ and H_2O^+ channels become close but do not cross (cf. Fig. 8 of Ref. [15]).

Also indicated in Fig. 5 is the Bethe-Born high-energy result based on the population ratios given in Eq. (36) of Ref. [15]. The full IPM-BGM calculations agree with this limit above 5 MeV/amu, as they should.

In Fig. 6 our fragmentation data are compared specifically for (a) the capture channel ($k = 2$), (b) the pure ionization channel ($k = 1$), and (c) the projectile electron loss channel ($k = 0$), which are evaluated using Eqs. (13), (14), and (15), respectively, in the fragmentation model (11). At high energies the theoretical cross sections for cases (a) and (c) display a more rapid fall-off than for (b). This happens because the $k = 2$ and $k = 0$ channels are suppressed for large impact parameters, which is not the case for pure ionization.

Concerning the comparison between the theory and experiment the following comments can be made.

(i) For the capture channel (a), the theory predicts H^+ production to dominate more than seen in the experiment; remarkably O^+ is equally strong to OH^+ above 100 keV/amu (in the experiment and in the theory), which underlines the role played by multiple electron removal in transfer ionization. Given the unusual energy dependence of the experimental data points it would be desirable to have more fragmentation measurements available for comparison, especially at lower impact energies where theoretical and experimental net capture cross sections are in very good agreement with each other (cf. Fig. 1).

(ii) For the pure ionization channel (b), the theory agrees with experiment rather well, and shows that this channel dominates the data displayed in Fig. 5.

(iii) In the projectile electron loss channel (c), the comparison is not as bad as one might have expected on the basis of Fig. 3: while the trend is clearly off for H_2O^+ production at high energies, the general agreement is reasonable for most singly charged ions at energies below 300 keV/amu. The production of H^+ is seen to be very strong between 100–200 keV/amu, and the OH^+ production is not much stronger than that of O^+. As in the capture channel this is the result of selecting small to intermediate impact parameters for which multiple electron events are not less likely than single-electron removal from the water molecule.

IV. CONCLUSION

We have carried out *ab initio* $(N + 1)$-electron calculations for He^+-H_2O collisions within the IPM-BGM. These calculations extend our previous work for proton-H_2O collisions [14–16], and treat the projectile electron on the same footing as the target electrons. Net cross sections from these calculations were compared to experiments at low and intermediate energies. As expected, the importance of multiple electron removal was found to be somewhat stronger than for proton projectiles.

A semiphenomenological fragmentation model developed previously for the proton projectile case was then applied to turn the theoretical data for q-fold electron removal into predictions for the production of singly charged fragments (H_2O^+,H^+,OH^+,O^+). A comparison with experimental data in the 100–500 keV/amu energy range [12] shows good agreement for the $k = 1$ channel (pure ionization); for the $k = 2$ (capture) and $k = 0$ (loss) channels we find that certain features of the experiment are reproduced correctly. Some details are lacking and require further understanding; particularly the evolution of the data toward higher energies in the projectile electron loss channel is not explained by the present theory.

ACKNOWLEDGMENTS

This work was supported by NSERC Canada and by SHARCNET.

[1] U. Werner, K. Beckord, J. Becker, and H. O. Lutz, Phys. Rev. Lett. **74**, 1962 (1995).

[2] F. Gobet, B. Farizon, M. Farizon, M. J. Gaillard, M. Carré, M. Lezius, P. Scheier, and T. D. Märk, Phys. Rev. Lett. **86**, 3751 (2001).

[3] Z. D. Pešić, J.-Y. Chesnel, R. Hellhammer, B. Sulik, and N. Stolterfoht, J. Phys. B **37**, 1405 (2004).

[4] H. Luna and E. C. Montenegro, Phys. Rev. Lett. **94**, 043201 (2005).

[5] B. Seredyuk, R. W. McCullough, H. Tawara, H. B. Gilbody, D. Bodewits, R. Hoekstra, A. G. G. M. Tielens, P. Sobocinski, D. Pesic, R. Hellhammer, B. Sulik, N. Stolterfoht, O. Abu-Haija, and E. Y. Kamber, Phys. Rev. A **71**, 022705 (2005).

[6] P. Sobocinski, Z. D. Pešić, R. Hellhammer, N. Stolterfoht, B. Sulik, S. Legendre, and J.-Y. Chesnel, J. Phys. B **38**, 2495 (2005).

[7] P. Sobocinski, Z. D. Pešić, R. Hellhammer, D. Klein, B. Sulik, J.-Y. Chesnel, and N. Stolterfoht, J. Phys. B **39**, 927 (2006).

[8] F. Gobet, S. Eden, B. Coupier, J. Tabet, B. Farizon, M. Farizon, M. J. Gaillard, S. Ouaskit, M. Carré, and T. D. Märk, Chem. Phys. Lett. **421**, 68 (2006).

[9] H. Luna, A. L. F. de Barros, J. A. Wyer, S. W. J. Scully, J. Lecointre, P. M. Y. Garcia, G. M. Sigaud, A. C. F. Santos, V. Senthil, M. B. Shah, C. J. Latimer, and E. C. Montenegro, Phys. Rev. A **75**, 042711 (2007).

[10] S. W. J. Scully, J. A. Wyer, V. Senthil, M. B. Shah, and E. C. Montenegro, Phys. Rev. A **73**, 040701(R) (2006).

[11] E. C. Montenegro, M. B. Shah, H. Luna, S. W. J. Scully, A. L. F. de Barros, J. A. Wyer, and J. Lecointre, Phys. Rev. Lett. **99**, 213201 (2007).

[12] P. M. Y. Garcia, G. M. Sigaud, H. Luna, A. C. F. Santos, E. C. Montenegro, and M. B. Shah, Phys. Rev. A **77**, 052708 (2008).

[13] K. H. Tan, C. E. Brion, P. E. van der Leeuw, and M. J. van der Wiel, Chem. Phys. **29**, 299 (1978).

[14] H. J. Lüdde, T. Spranger, M. Horbatsch, and T. Kirchner, Phys. Rev. A **80**, 060702(R) (2009).

[15] M. Murakami, T. Kirchner, M. Horbatsch, and H. J. Lüdde, Phys. Rev. A **85**, 052704 (2012).
[16] M. Murakami, T. Kirchner, M. Horbatsch, and H. J. Lüdde, Phys. Rev. A **85**, 052713 (2012).
[17] H. J. Lüdde and R. M. Dreizler, J. Phys. B **18**, 107 (1985).
[18] T. Kirchner and M. Horbatsch, Phys. Rev. A **63**, 062718 (2001).
[19] T. Kirchner, M. Murakami, M. Horbatsch, and H. J. Lüdde, J. Phys.: Conf. Ser., (to be published).
[20] S. Aung, R. M. Pitzer, and S. I. Chan, J. Chem. Phys. **49**, 2071 (1968).
[21] T. Kirchner, A. C. F. Santos, H. Luna, M. M. Sant'Anna, W. S. Melo, G. M. Sigaud, and E. C. Montenegro, Phys. Rev. A **72**, 012707 (2005).
[22] M. E. Rudd, A. Itoh, and T. V. Goffe, Phys. Rev. A **32**, 2499 (1985).
[23] M. E. Rudd, T. V. Goffe, A. Itoh, and R. D. DuBois, Phys. Rev. A **32**, 829 (1985).
[24] M. Sakata, A. Yagishita, and Y. Nakai, J. Phys. B **23**, 1225 (1990).
[25] M. E. Rudd, Y.-K. Kim, D. H. Madison, and J. W. Gallagher, Rev. Mod. Phys. **57**, 965 (1985).
[26] E. C. Montenegro, W. E. Meyerhof, and J. H. McGuire, Adv. At. Mol. Opt. Phys. **34**, 249 (1994).
[27] E. Montenegro, J. Phys.: Conf. Ser. **194**, 012049 (2009).